TISSUE ENGINEERING: Part A
Volume 17, Numbers 17 and 18, 2011

DOI: 10.1089/ten.tea.2010.0682

A Tissue-Engineered Muscle Repair Construct for Functional Restoration of an Irrecoverable Muscle Injury in a Murine Model

Masood A. Machingal, Ph.D.,[1,2] Benjamin T. Corona, Ph.D.,[1] Thomas J. Walters, Ph.D.,[3] Venu Kesireddy, Ph.D.,[1] Christine N. Koval, B.S.,[1] Ashley Dannahower, B.S.,[1] Weixin Zhao, M.D.,[1] James J. Yoo, M.D.,[1,2] and George J. Christ, Ph.D.[1,2]

There are no effective clinical treatments for volumetric muscle loss (VML) resulting from traumatic injury, tumor excision, or other degenerative diseases of skeletal muscle. The goal of this study was to develop and characterize a more clinically relevant tissue-engineered muscle repair (TE-MR) construct for functional restoration of a VML injury in the mouse lattissimus dorsi (LD) muscle. To this end, TE-MR constructs developed by seeding rat myoblasts on porcine bladder acellular matrix were preconditioned in a bioreactor for 1 week and implanted in nude mice at the site of a VML injury created by excising 50% of the native LD. Two months postinjury and implantation of TE-MR, maximal tetanic force was ~72% of that observed in native LD muscle. In contrast, injured LD muscles that were not repaired, or were repaired with scaffold alone, produced only ~50% of native LD muscle force after 2 months. Histological analyses of LD tissue retrieved 2 months after implantation demonstrated remodeling of the TE-MR construct as well as the presence of desmin-positive myofibers, blood vessels, and neurovascular bundles within the TE-MR construct. Overall, these encouraging initial observations document significant functional recovery within 2 months of implantation of TE-MR constructs and provide clear proof of concept for the applicability of this technology in a murine VML injury model.

Introduction

Mammalian skeletal muscle has a rather remarkable capacity for repair after a variety of injuries. Typically, muscle injury or damage is followed by an inflammatory response, resulting in a cycle of degeneration, repair/regeneration, and remodeling (see reviews[1–3]). Satellite cells represent the major stem cell source required for repair and remodeling although clearly other stem and progenitor cell populations may participate in the regenerative response as well.[4–9] Nonetheless, there are a host of traumatic injuries, as well as congenital and acquired diseases and disorders, that result in a significant loss of muscle function that cannot be effectively compensated by intrinsic regenerative mechanisms. A particularly striking example is the complex soft tissue battlefield injuries suffered by military personnel. In fact, although the battle mortality rate for U.S. forces wounded in combat has dropped from 30% in WWII to less than 10% in Afghanistan and Iraq,[10] there has been a parallel increase in the number of seriously injured soldiers who survive with extraordinary injuries; especially complex and severe extremity and head/neck injuries.[11–13] Analogous injuries are observed after traumatic accidents and gunshot wounds in civilians. Such injuries are characterized by volumetric muscle loss (VML)[14] and are associated with devastating cosmetic and functional deficits.

In this regard, current management of VML injuries involves the use of existing host tissue to construct muscular flaps or grafts (see reviews[15,16]). However, even when sufficient graft tissue exists, this approach is associated with significant donor-site morbidity,[17,18] thus delaying rehabilitation and restoration of tissue function. Moreover, when this approach is not feasible, the patient is left with a high level of morbidity, permanent functional disfigurement, and the associated loss of quality of life and self-esteem. In this scenario, the ability to create a clinically relevant autologous tissue-engineered muscle repair (TE-MR) construct would remove a major hurdle to the successful skeletal muscle reconstructive procedures required to repair complex extremity and facial injuries suffered by both soldiers and civilians.

In this regard, tissue engineering and regenerative medicine technologies have the potential to provide groundbreaking

[1]Wake Forest Institute for Regenerative Medicine, Wake Forest University Baptist Medical Center, Winston Salem, North Carolina.
[2]Virginia Tech-Wake Forest University School of Biomedical Engineering and Sciences, Winston Salem, North Carolina.
[3]U.S. Army Institute of Surgical Research, San Antonio, Texas.

autologous therapies for functional reconstruction and restoration of such complex injuries (for recent review see Koning *et al.*[19]). Indeed, significant progress has been made during the last 20 years in describing some of the basic requirements for creating tissue-engineered skeletal muscle constructs.[20–24] To this end, three distinct preclinical strategies are currently being developed for creation of engineered muscle tissue for functional reconstruction/restoration of VML injuries. The first involves the implantation of a scaffold alone at the site of injury, and this is referred to as the acellular approach.[25–29] Badylak and colleagues have reported that after 6 months, the implantation of a biocompatible small intestinal submucosa (SIS) extracellular matrix scaffold to the site of a VML musculotendinous injury in dogs resulted in scaffold-localized tissue formation that exhibited the ability to contract when directly stimulated *in vitro*.[25] Similar results were obtained with SIS implantation in a rodent abdominal wall VML injury *in situ*.[26] In a second approach, Merritt *et al.* reported that a surgical defect in the rat gastrocnemius muscle resulted in an initial ~25% reduction in force.[29] While a decellularized muscle matrix did not facilitate functional recovery up to 42 days post-injury,[29] injection of mesenchymal stem cells into the scaffold 7 days after creation of a surgical defect led to functional recovery to ~85% of contralateral muscle force at 42 days, as assessed by neural stimulation.[30]

The subject of this report focuses on a third approach, that is, the use of a tissue engineering strategy in which muscle progenitor cells (MPCs) are seeded on a biocompatible bladder accellular matrix (BAM) and preconditioned in a bioreactor *in vitro* before implantation *in vivo*. Previous work documented the importance of such *in vitro* bioreactor preconditioning to engineered skeletal muscle tissue formation and function after subcutaneous implantation *in vivo*.[31] The current report builds logically on this prior work to illustrate how this tissue engineering strategy can be used to promote *in vivo* functional restoration of a skeletal muscle with VML injury. Specifically, to simulate the repair required in a VML injury setting, we conducted a proof-of-concept study in which we implanted an allogeneic TE-MR construct into mouse latissimus dorsi (LD) muscle after surgical removal of ~50% of the muscle.

Materials and Methods

Cell isolation and culture

MPCs were isolated from surgical biopsies obtained from the soleus and tibialis anterior muscles of male Lewis rats (Charles River). The muscles were isolated in a sterile fashion and washed once with iodine followed by two washes with sterile PBS. Muscles were then cut into small pieces and incubated in 0.2% collagenase (Worthington Biochemicals) solution prepared in low glucose Dulbecco's modified Eagle's medium (DMEM; Hyclone) for 2 h 37°C. Muscle tissue fragments were plated onto tissue culture dishes coated with Matrigel (BD Biosciences) in myogenic medium containing: DMEM high glucose supplemented with 20% fetal bovine serum (FBS), 10% horse serum, 1% chicken embryo extract, and 1% antibiotic/antimycotic (Hyclone). Cells were passaged at 60%–70% confluence, cultured in low-glucose DMEM supplemented with 15% FBS and 1% antibiotic/antimycotic, and used for seeding at the first or second passage.

Preparation of BAM

BAM scaffolds were prepared from porcine urinary bladder as previously described.[31] Briefly, the bladder was washed and trimmed to obtain the lamina propria, which was placed in 0.05% Trypsin (Hyclone) for 1 h at 37°C. The bladder was then transferred to DMEM solution supplemented with 10% FBS and 1% antibiotic/antimycotic and kept over night at 4°C. The preparation was then washed in a solution containing 1% Triton X (Sigma-Aldrich) and 0.1% ammonium hydroxide (Fisher Scientific) in de-ionized water for 4 days at 4°C. Finally, the bladder was then washed in de-ionized water for 3 days at 4°C. The absence of cellular elements and preservation of structural components was confirmed by histological assessments (Fig. 1D, E). The decellularized scaffold was further dissected to obtain a scaffold with of 0.3–0.4 mm thickness; dimensions suitable for implantation in the surgically created mouse LD defect. The prepared acellular matrix was then cut into strips of 3×2 cm size and placed onto a custom-designed seeding chamber made of silicon (McMaster Carr). Scaffolds and silicon seeding chambers were then individually placed in six-well culture dishes and sterilized by ethylene oxide (Fig. 1F).

Cell seeding and bioreactor preconditioning

Sterilized scaffolds in the custom-designed seeding chambers were kept immersed in DMEM solution supplemented with 10% FBS and 1% penicillin/streptomycin media for at least 12 h at 37°C before seeding. MPCs were then seeded at a concentration of 1 million cells per cm^2, and after 12 h, the seeding chamber was flipped and a concentration of 1 million cells per cm^2 was seeded on the other side. Both cell-seeded surfaces (i.e., top and bottom of the same BAM scaffold) were fully immersed in media during the entire seeding process. On day 4, the medium was changed to differentiation medium (F12 DMEM, 2% horse serum, 1% antibiotic/antimylotic) and the cells were cultured for an additional 7 days. After a total of 10 days of static culture, the cell-seeded scaffolds (i.e., TE-MR constructs) were then placed in the bioreactor system as described previously.[31] The bioreactor system consisted of a computer-controlled linear motor powered actuator for providing cyclic unidirectional stretch and relaxation. To permit application of the cyclic stretch protocol, one end of the TE-MR construct was attached to a stationary bar, whereas the other end was connected to a movable bar attached to the actuator. TE-MR were subjected to 10% stretch, three times per minute for the first 5 min of every hour, for 1 week (see Moon *et al.*[31] for details). The tissue constructs were continuously aerated with 95% air–5% CO_2 at 37°C in an incubator, and the medium was changed every 3 days.

Scanning electron microscopy and fluorescent microscopy assessment of TE-MR constructs

Scanning electron microscopy (SEM) imaging was performed to evaluate the cellular coverage on the BAM before and 7 days after static seeding with MPCs. For these studies, scaffolds were fixed in 2.5% gluteraldyhyde for 2 h and stored in 70% ethanol until used. Samples were freeze-dried in a lyophilizer and sputter-coated and observed through SEM (Model S-2260N; Hitachi). Quantification of the scaffold

area covered by cells was performed on SEM images using Image Pro software. In addition, after bioreactor preconditioning BAM scaffolds were imaged in whole mount fashion using a fluorescent microscope (DM4000B Leica Upright Microscope; Leica Microsystems). For these studies, scaffolds were transferred to a slide, washed with PBS, fixed in 2% formalin, and permeabilized in 0.5% Triton. After blocking (5% nonfat milk; 30 min), the scaffold was incubated for 1 h at room temperature in the dark with desmin antibody (Santa Cruz-7995; goat polyclonal) and phalloidin (rhodamine; conjugated TRITC; Invitrogen-R415). The scaffold was then washed with PBS (3 × 5 min), and incubated in a desmin secondary antibody (fluorescein rabbit anti-goat; Vector-FI-5000) for 30 min in the dark. Whole mount specimens were then cover-slipped with ProLong Gold including DAPI (Invitrogen–P36931).

Animal care

This study was conducted in compliance with the Animal Welfare Act, the Implementing Animal Welfare Regulations, and in accordance with the principles of the Guide for the Care and Use of Laboratory Animals. The Wake Forest University Health Sciences School of Medicine Animal Care and Use Committee approved all animal procedures. Adult female nu/nu mice weighing 20–25 g (Harlan Laboratories) were individually housed in a vivarium accredited by the American Association for the Accreditation of Laboratory Animal Care, and provided with food and water *ad libitum*.

Development of VML injury model

The VML injury model was created by surgically excising ~50% of the LD muscle area in anesthetized nu/nu mice. A longitudinal incision was made along the midline of the back. The trapezius muscle that covers the LD muscle was lifted to expose the LD muscle without removing the tendon inserted at the humerus. Suture markers were then placed on the LD muscle demarcating the superior half of the spinal fascia and the medial half of the of the muscle head at the humerus. The medial half of the muscle was then excised using a fine scissor (Fig. 1L). Using this methodology, a defect weighing ~25 ± 5 mg is retrieved, comprising ~45% ± 5% of whole LD muscle wet weight. After surgical excision, animals were placed into one of three treatment groups: (1) no repair (NR), (2) repair with TE-MR implantation (R-TE-MR), or (3) repair with implantation of BAM scaffold alone (R-S; i.e., no cells) at the excised sites (see Fig. 1M). The skin was then closed and the animals were allowed to recover. One or 2 months postimplantation animals were sacrificed and the LD muscle from animals in one of the three treatment groups, as well as the contralateral control LD muscle were retrieved for functional (i.e., contraction) or histological evaluation.

Physiological studies

The entire LD muscle was isolated from the thoracolumbar fascia to the humeral tendon of mice under anesthesia and quickly transferred into Krebs-Ringer buffer solution (composition: pH 7.4; concentration in mM: 121.0 NaCl, 5.0 KCl, 0.5 $MgCl_2$, 1.8 $CaCl_2$, 24.0 $NaHCO_3$, 0.4 NaH_2PO_4, and 5.5 glucose) in a 15 mL Radnoti organ bath continuously bubbled with 95% O_2 and 5% CO_2 at 28°C. Briefly, 5-0 silk suture was used to attach the humeral tendon to a force transducer (MLT0201/D; AD Instruments) mounted on a micromanipulator while the thoracolumbar fascia was attached to a static glass hook at the bottom of the organ bath (Radnoti model 160151; Monrovia). Electrical field stimulation (EFS) (20 Volts at electrodes, 0.2 ms square pulse, 1200 ms train) was applied to the muscle using parallel platinum electrodes. After a 10-min equilibration, optimal length was identified based on the twitch response, which was determined by adjusting the length of the muscle through rotation of the micrometer head. Peak isometric contractile force was measured at optimal length with a 1200 ms train of 0.2 ms pulses over a range of frequencies (1–150 Hz). Electrical stimulation was provided to the isolated muscle tissue by a stimulator (model S48; Grass Instruments). Real-time display and recording of all force measurements were performed on a PC with Power Lab/8sp (AD Instruments).

Pharmacological studies

A subset of LD muscles underwent a secondary caffeine contracture force assessment after the force-frequency measurements. For these studies, a maximal caffeine-induced contracture response was elicited by exposing the muscle to 50 mM caffeine during twitch contractions at 0.2 Hz.[32] This concentration of caffeine was chosen because concentrations in this (mM) range have been previously shown to maximally stimulate whole uninjured and injured rodent skeletal muscle.[32–34] During this testing, resting tension of the muscle increases until active force and resting tension are indistinguishable and then the response plateaus. Peak caffeine contracture force was defined as the tension measured at this steady-state response. The scientific rationale for performing a caffeine contracture test is that caffeine directly stimulates the sarcoplasmic reticulum (SR) to release Ca^{2+}, thereby bypassing upstream components of the voltage-induced SR Ca^{2+} release process (i.e., excitation–contraction coupling).[35–37] Thus, regenerating fibers that have the requisite contractile machinery and SR Ca^{2+} load but have yet to completely develop mature E-C coupling structures may contribute to caffeine-induced force and not voltage-induced force.

Histology and immunochemistry

After organ bath experiments, retrieved tissues were fixed in 10% neutral buffered formalin and stored in 60% ethanol. Next, all specimens were placed in the tissue processor (ASP300S; Leica Microsystems) and then embedded in paraffin (EG1160; Leica Microsystems). Seven-micrometer-thick serial sections were cut from the paraffin-embedded blocks and staining with hematoxylin and eosin (H&E) and Herovici polychrome was performed. Immunohistochemical studies were performed on retrieved tissues with skeletal muscle-specific anti-Desmin (M0760, 1:75; Dako), anti–Von Willebrand factor (vWF, A0082, 1:200; Dako), and anti-Neurofilament 200 (N4142, 1:300; Sigma-Aldrich) according to the manufacturer's guidelines. The corresponding secondary antibodies used were biotinylated anti-mouse IgG (MKB-2225, 1:250; Vector Laboratories, Inc.), biotinylated goat anti-rabbit (BA-1000, 1:500; Vector Laboratories, Inc.), and biotinylated goat anti-rabbit (BA-1000, 1:300; Vector Laboratories, Inc.). The sections were next treated with Avidin Biotin Complex Reagent (PK-7100; Vector Laboratories,

Inc.) and then observed using a NovaRED substrate kit (SK-4800; Vector Laboratories, Inc.). Finally, the sections were counterstained using Gill's hematoxylin (GHS280; Sigma-Aldrich). Tissue sections without primary antibody were used as negative controls. Images were captured and digitized (DM4000B Leica Upright Microscope; Leica Microsystems) at varying magnifications. Quantification of desmin-positive cells for the R-TE-MR and R-S groups 2 months postimplantation was performed by counting the number of desmin-positive cells expressed as a percentage of total cells in each 400× high power field. This quantification was performed at two different locations, (1) at the interface of LD and implant and (2) within the implant, ~450–500 μm from the interface. Similarly, the number of vessels in each high power field were counted and expressed as the number of vessels per scaffold area in R-TE-MR and R-S groups 2 months postimplantation at the two locations described above (see Fig. 4A).

Data analysis and statistics

Force was expressed as force generated (mN) or as force normalized to physiological cross-sectional area (PCSA) (i.e., specific force mN/mm^2). Before detachment from the organ bath, the length of the muscle was determined using a digital micrometer; the muscle was then detached, blotted dry, and weighed. These values were used to determine PCSA according to the following formula: PCSA = mass/(density × muscle length), where density is $1.06\,g/cm^3$.[38]

Unless otherwise stated, all data were presented as the arithmetic mean ± standard error of the mean. One-way ANOVAs were performed at each frequency for EFS-induced forces, as well as for the caffeine contracture experiments and all LD muscle morphological measures (e.g., weight). When ANOVA analysis revealed a significant difference, a Fischer LSD *post hoc* test was performed. Group wise quantitative histological analysis (Desmin percentage and vascularization) between R-TE-MR and R-S was performed by unpaired t test. In all cases, the statistical significance level was set at $\alpha = 0.05$. All statistical analyses were performed using SPSS software.

Results

Evaluation of tissue organization in vitro

The phenotype of the MPCs before cell seeding and bioreactor preconditioning was evaluated by immunohistochemical staining. Positive immunostaining was observed for Myo-D, desmin, and myosin. MPCs were seeded on the BAM scaffold and placed in a custom-made seeding chamber. Cellular attachment, phenotype, and tissue organization on BAM were further analyzed with immunofluorescence and SEM (Fig. 1). SEM imaging demonstrated cellular coverage of ~95% of the scaffold surface area after 7 days of static seeding. Representative SEM images of an unseeded BAM scaffold as well as presumptive myotube formation after 7 days are shown in Figure 1G and J, respectively. After static seeding, constructs were preconditioned in a bioreactor for 1 week and immunostaining was performed with phalloidin (Fig. 1H) to observe the cytoskeleton and desmin (Fig. 1I). Aligned multinucleated (stained with DAPI) myotubes were observed on these TE-MR constructs after bioreactor preconditioning. The macroscopic characteristics of the implanted TE-MR are also depicted in Figure 1K–M.

Creation of VML injury and morphological assessment of retrieved tissue

A VML injury was created by surgically excising ~50% of the native LD (Fig. 1L). After surgical excision, animals were placed into one of three treatment groups: (1) no repair (NR), (2) TE-MR implantation (R-TE-MR, Fig. 1K, M), or (3) implantation of BAM scaffold alone (R-S; i.e., no cells) at the excised sites. In all cases the NR, R-TE-MR, or R-S muscles were retrieved along with the corresponding contralateral native LD muscle at either 1 or 2 months after implantation. Figure 2 shows representative images of retrieved tissues in the NR (Fig. 2A) and R-TE-MR (Fig. 2B) treatment groups 2 months postimplantation. As illustrated, the TE-MR construct was well integrated into native LD muscle with evidence of a vascular network on the repaired side of the LD muscle.

Physiological studies of contractile force generation

To evaluate the recovery of force generation in retrieved muscle, EFS-induced tetanic contractile responses were obtained for the native LD, NR, R-TE-MR, and R-S groups to varying EFS frequencies (10–150 Hz). Individual tracings from R-TE-MR and native LD for EFS responses at 10, 30, 60, and 120 Hz are shown in Figure 3A and B, respectively. Consistent with the gross morphological observations, the force responses revealed evidence for significant functional recovery 2 months postimplantation. Force–frequency relationships observed in all animals studied are summarized at the 1-month (Fig. 3C) and 2 month (Fig. 3D–F) time points postimplantation.

As shown, absolute maximal isometric tetanic force generated by muscle retrieved 1 month postimplantation from the NR group was significantly smaller than that of native LD muscle (100.7 ± 16.2 vs. 309.3 ± 12.7 mN, respectively; $p < 0.05$). Force generated by LD muscles of the R-TE-MR, 1 month postimplantation was 149.8 ± 23.2 mN, or 48% of native LD muscle, but not statistically different from muscles of the NR group ($p = 0.10$). However, 2 months postimplantation, force generation was significantly greater in muscles of the R-TE-MR (222.5 ± 21.7 mN) than the NR group (139.0 ± 25.3 mN), with the former generating ~72% of maximal force produced by native LD muscle ($p < 0.05$). Additionally, muscles of the R-TE-MR group retrieved 2 months postimplantation generated significantly greater ($p < 0.05$) force than muscle tissue retrieved from the R-S group (143.5 ± 15.7 mN) at the same time point, indicating that implantation of the scaffold alone (i.e., in the absence of cells) does not result in significant functional recovery in this model, at this time point. Consistent with this observation, the magnitude of force generation by muscles of the R-S and NR groups was statistically indistinguishable ($p > 0.05$).

Similar results were observed when isometric tetanic force was normalized to PCSA (i.e., specific force; Fig. 3E). More specifically, maximal isometric specific force for native LD muscle was 150.8 ± 4.8 mN/mm^2, which was similar to that reported previously by our group.[31] Maximal specific isometric force for the NR group one and 2 months postimplantation, respectively, was 47.3 ± 6.2 (31% of native) and 69.5 ± 10.4 (46% of native) mN/mm^2. The specific force of the retrieved

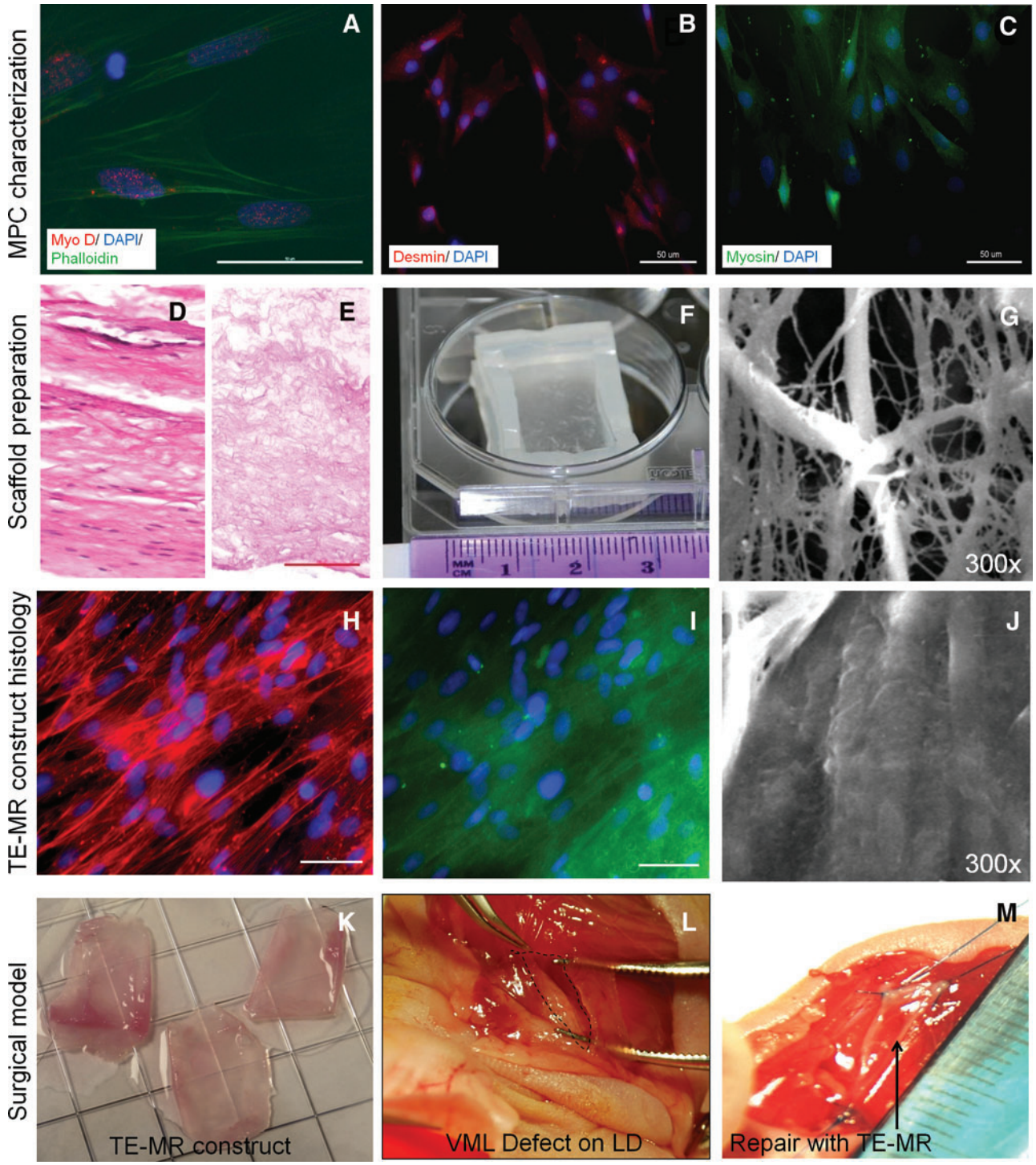

FIG. 1. Development and *in vitro* assessment of tissue-engineered muscle repair (TE-MR) constructs. Immunofluoresence imaging of muscle progenitor cells (MPCs) **(A–C)** indicates the presence of muscle-specific markers such as myo-D **(A)**, desmin **(B)** and myosin **(C)**. Preparation of bladder acellular matrix (BAM) scaffold is shown in **(D–F)**. Representative cross-sectional hematoxylin and eosin images of native porcine bladder **(D)** before and after and decellularization **(E)** indicate the absence of cellular materials in the scaffold and preservation of the extracellular matrix (scale bar = 100 μm). After the decellularization process, the BAM scaffolds were placed on a custom-made seeding chamber **(F)** and seeded with MPCs. Scanning electron microscopy imaging was performed to evaluate the cellular coverage on the BAM before **(G)** and 7 days after static seeding **(J)** with MPCs. Myotube formation and cellular coverage were observed on ~95% of the BAM scaffold surface area. Immunostaining with phalloidin **(H)** and desmin **(I)** demonstrates the aligned multinucleated (DAPI) myofibers in a bioreactor preconditioned TE-MR construct (scale bar 50 μm). TE-MR constructs after bioreactor preconditioning **(K)** were implanted in a volumetric muscle loss (VML) injury model in mice. VML injury was developed by excising ~50% of the native lattissimus dorsi (LD) resulting in a volumetric muscle defect **(L,** excised area indicated by black dotted lines**)**. The defect was repaired by suturing either TE-MR constructs or scaffolds without cells at the site of excised sites **(M;** arrow points to implant**)**. Color images available online at www.liebertonline.com/tea

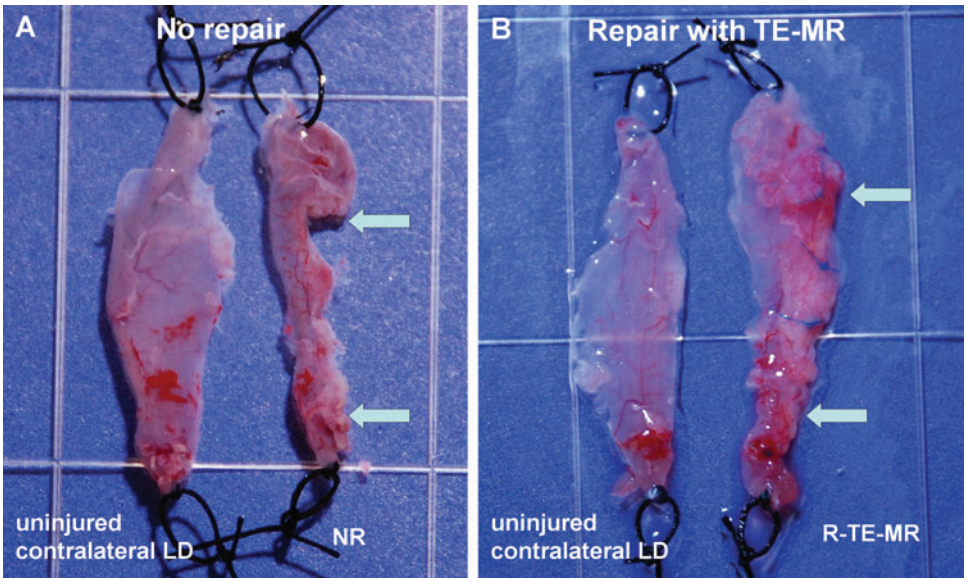

FIG. 2. Morphological assessment of retrieved tissues from the no repair (NR; **A)** and repair (R-TE-MR; **B)** treatment groups, compared to the contralateral LD 2 months after implantation. Arrows indicate the original site of the surgical defect. Morphological examination of tissue demonstrates robust tissue formation and remodeling of the TE-MR construct, but little or no tissue formation in the NR group. Color images available online at www.liebertonline.com/tea

R-TE-MR demonstrated a time-dependent increase from $33.6 \pm 8.6\,mN/mm^2$ (22% of native) at the 1-month time point to a mean value of $99.2 \pm 17.7\,mN/mm^2$ at 2 months, with the latter being 66% of the native LD muscle isometric specific force. Isometric specific force of the R-S group was $45.20 \pm 3.83\,mN/mm^2$, only ~30% of native LD muscle isometric force 2 months postimplantation. Moreover, the specific force of the R-TE-MR group was significantly greater than that observed for all other treatment groups, but was still significantly lower than native LD muscle ($P < 0.05$ in all cases). A summary of the mean *in vitro* specific force data for all treatment groups, along with their respective length and wet weight measurements is provided in Table 1. In this regard, muscle lengths among all groups were similar, however, the R-TE-MR retrieved 1 month postimplantation weighed (wet weight) significantly more than all other groups, consistent with a corresponding time-dependent scaffold degradation.

Pharmacological studies

Maximal caffeine contracture force was also measured for a subset of muscles retrieved 2 months postimplantation (Fig. 3F). Specific contracture force (mN/mm^2) produced by the NR ($n = 4$) and R-S ($n = 4$) groups was significantly reduced to only ~34 and 30%, respectively, of control LD values ($n = 6$). Implantation of TE-MR constructs (R-TE-MR; $n = 3$) resulted in a significant recovery of caffeine contracture to ~71% compared to control values (Fig. 3F). The ratio of caffeine contracture to peak isometric voltage-induced force, an index of excitation-contraction coupling,[36] was significantly greater ($p < 0.05$) for injured LD muscles repaired with TE-MR constructs (0.38 ± 0.05) than uninjured (0.23 ± 0.04) and injured LD muscles with no repair (0.28 ± 0.05) or scaffold-only repair (0.31 ± 0.03).

Histological and immunochemical characterization of retrieved tissue

Histological and immunohistochemical methods were used to evaluate the cellularity, extent of scaffold remodeling, and presence of vasculature and neuronal innervation in retrieved tissue 2 months postimplantation. As shown in Figure 4, this investigation focused on analysis of longitudinal sections of retrieved tissues, parallel to the native LD and implant (either R-TE-MR construct) or scaffold alone (R-S group)). In this regard, desmin-positive striated myofibers (Fig. 4B) and multinucleated myotubes were present at the interface of native LD and R-TE-MR (Fig. 4C; shown by black arrowheads) as well as inside the TE-MR scaffold (Fig. 4D; black arrowheads). Similarly, individual presumptive myoblasts were also observed within the construct (white arrows, Fig. 4D).

Figure 5 demonstrates the significant remodeling of the TE-MR construct, with a focus on highlighting the formation of vasculature (Fig. 5A, D) and innervation (Fig. 5C). Again, immunohistological staining with desmin (Fig. 5A: 100× & B: 400×) indicates the presence of myofibers (black arrowheads) and blood vessels (white arrowheads) within the TE-MR construct. NF 200 staining (Fig. 5C) indicates the presence of nerve fibers at the interface of the native LD and the TE-MR. Further evidence of remodeling was observed with Herovici polychrome staining clearly demonstrating the formation of new collagen (blue) within the TE-MR (mature collagen from scaffold is shown in red), again at the interface with the native LD (Fig. 6A). We also observed neurovascular bundles stained with NF200 and vWF (Fig. 6B, C).

Quantitative immunohistochemical analysis of the aforementioned sections from retrieved tissue shows that the R-TE-MR group had a significantly greater percentage of desmin-positive cells when compared to the R-S treatment group—both in the LD-TE construct interface ($46.2\% \pm 2.9\%$ vs. $33.9\% \pm 1.5\%$) as well as within the implant ($46.4\% \pm 3.4\%$ vs. $29.8\% \pm 1.6\%$) (Fig. 7A). Additionally, new blood vessels were observed as demonstrated by vWF staining of endothelial cells near the implant interface as well as inside the TE-MR construct. In short, the number of vessels observed was significantly greater in R-TE-MR than that of R-S—both near the interface (11.6 ± 3.3 vessels/mm^2 vs. 2.3 ± 0.9 vessels/mm^2) and within the TE-MR construct (8.8 ± 2.6 vessels/mm^2 vs. 0.7 ± 0.4 vessels/mm^2) (Fig. 7B).

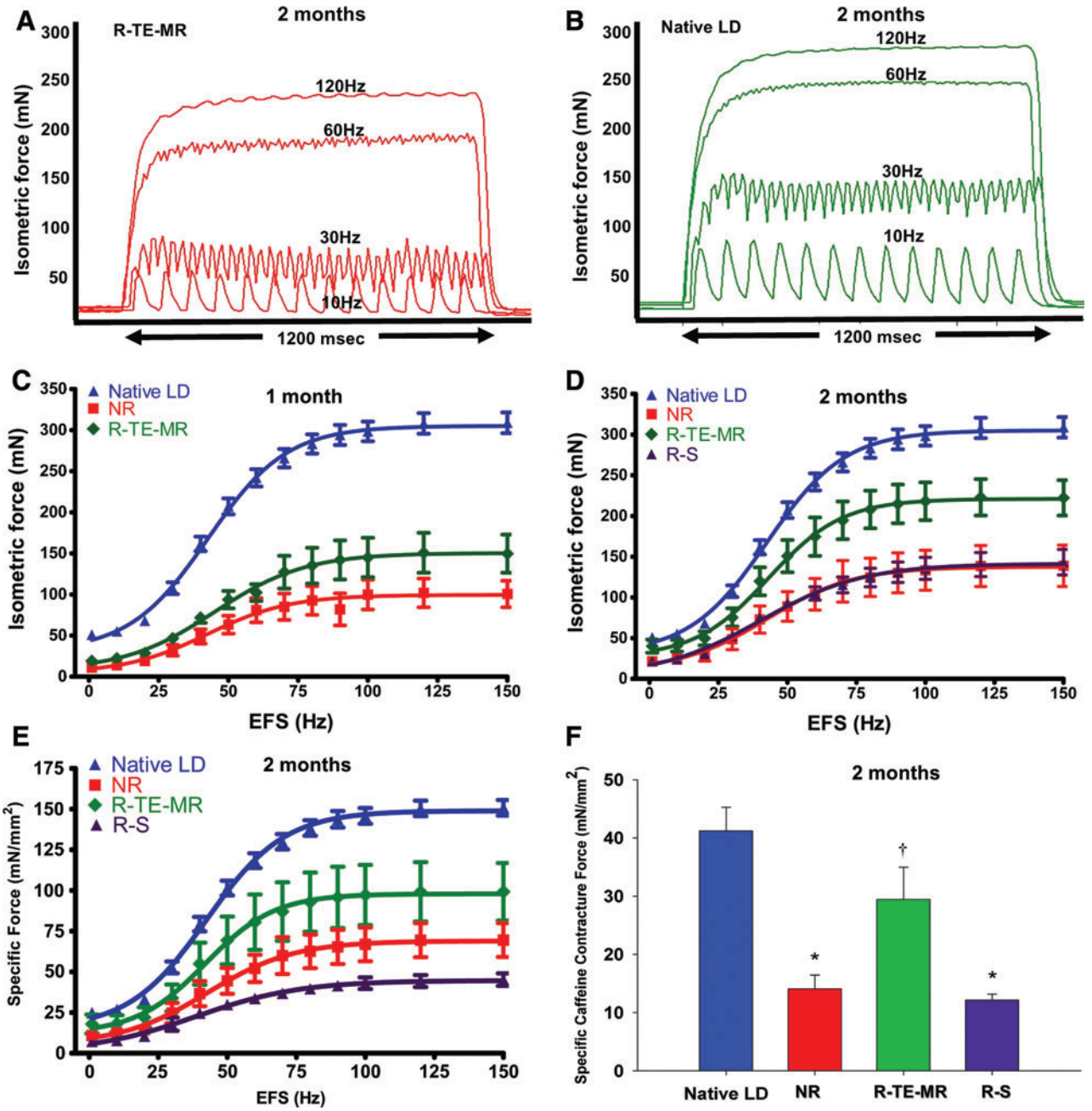

FIG. 3. Functional recovery of injured LD after implantation of TE-MR construct. Representative tracings showing the isometric contractions elicited in response to electrical field stimulation (EFS) frequencies of 10, 30, 60, and 120 Hz by R-TE-MR **(A)** assessed *in vitro* 2 months after implantation and by uninjured contralateral LD muscle **(B)**. The mean values for the EFS-induced contractions observed on all retrieved tissues in each study group are depicted for both the 1 month **(C,** *n*: native LD = 20, NR = 7, R-TE-MR = 6**)** and 2 month **(D,** *n*: native LD = 20, NR = 5, R-TE-MR = 5 and R-S = 5**)** time points, as expressed in both isometric absolute force **(**mN; **C&D)**, and specific force as a function of stimulation frequency **(E,** *n*: native LD = 20, NR = 5, R-TE-MR = 4 and R-S = 5**)**. Additionally, after force-frequency testing contralateral native LD muscles ($n = 6$), NR ($n = 4$), R-TE-MR ($n = 3$), or R-S ($n = 4$) at the 2 month time point were subjected to twitch contractions at 0.2 Hz in the presence of a maximally stimulating concentration of caffeine (50 mM) and **(F)**. *Group means are significantly different from that of control ($p < 0.05$). Values are means ± standard error of the mean. †Group mean is significantly different from that of all other groups ($p < 0.05$). Color images available online at www.liebertonline.com/tea

Discussion

Herein, we report the results of our most recent studies for the continued preclinical development of a TE-MR technology designed to restore function to skeletal muscle after a VML injury. As a first step in this direction, we created a VML injury model in mice by surgically excising ~50% of the LD muscle, which corresponded to a more than 50% decline in absolute maximal tetanic force 1 month after injury. Further, this injury exhibited little or no functional

Table 1. Lattissimus Dorsi Summary of Lattissimus Dorsi Muscle Measurements and Force Generation *In Vitro*

Group	*Native*	*NR*	*R-TE-MR*	*NR*	*R-TE-MR*	*R-S*
Time point		1 month			2 months	
Sample size	20	7	6	5	4	5
Muscle length (mm)	36.4 ± 0.9	31.0 ± 1.7	33.7 ± 1.7	36.2 ± 2.2	35.4 ± 1.4	35.4 ± 1.8
Wet weight (mg)	80.6 ± 4.9	65.7 ± 11.5	184.7 ± 27.9[a]	74.1 ± 2.9	88.8 ± 2.9	120.8 ± 14.2[b]
PCSA (mm^2)	2.33 ± 0.11	2.27 ± 0.39	5.86 ± 0.88[a]	2.21 ± 0.20	2.67 ± 0.13	3.62 ± 0.40[b]
Specific force (mN/mm^2)	150.8 ± 4.8[a]	47.3 ± 6.2	33.6 ± 8.6	69.5 ± 10.4	99.2 ± 17.7[a]	45.2 ± 3.8

Values are expressed as the arithmetic mean ± standard error of the mean. $p < 0.05$ was considered significant in all cases.
[a]Significant difference from corresponding values for all other groups.
[b]Significant difference from corresponding values for all groups except R-TE-MR at 2 month.
PCSA, physiological cross-sectional area; TE-MR, tissue-engineered muscle repair; NR, no repair.

recovery 1 to 2 months postinjury in the absence of implantation of TE-MR (Fig. 3C, D). While other *in vivo* skeletal muscle injury models (e.g., mechanical or thermal injury) have induced force deficits of similar magnitude within the first few days after injury, in contrast to the VML injury model described here, these functional deficits were completely restored within ~1 month postinjury.[39–41] Thus, the nearly complete absence of endogenously mediated functional recovery over this time frame makes this an attractive model for identifying potentially applicable therapies for devastating trauma suffered by soldiers and civilians.

In this regard, implantation of a TE-MR construct (i.e., after bioreactor preconditioning of an MPC-seeded BAM scaffold) into a surgically created VML injury was associated

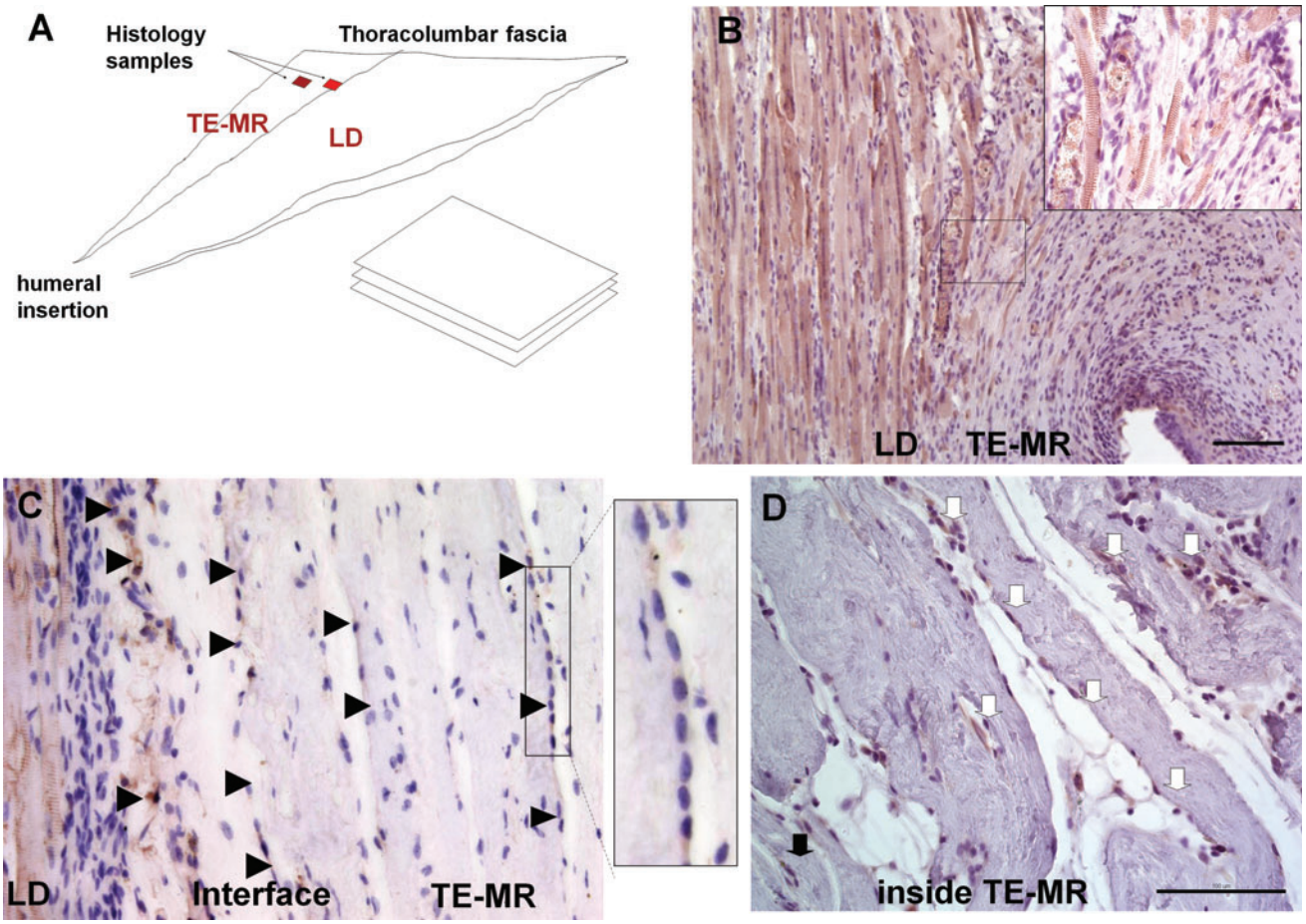

FIG. 4. Remodeling of TE-MR constructs and muscle tissue formation after implantation *in vivo*. **(A)** Schematic diagram of histological sample preparation from the explanted tissue indicating the location of native LD muscle and TE-MR construct, as well as the sample analysis paradigm. Immunohistological staining with desmin shows the presence of striated desmin-positive muscle fibers formed at the LD-TE-MR interface **(B)**. Desmin-positive multinucleated myotubes (black arrowheads) were also observed at the LD-TE-MR interface as well as within the TE-MR construct (~450–500 μm from interface) **(C)**. Desmin-positive myoblasts (white arrows) were also observed within the construct **(D)**. All scale bars = 100 μm. Color images available online at www.liebertonline.com/tea

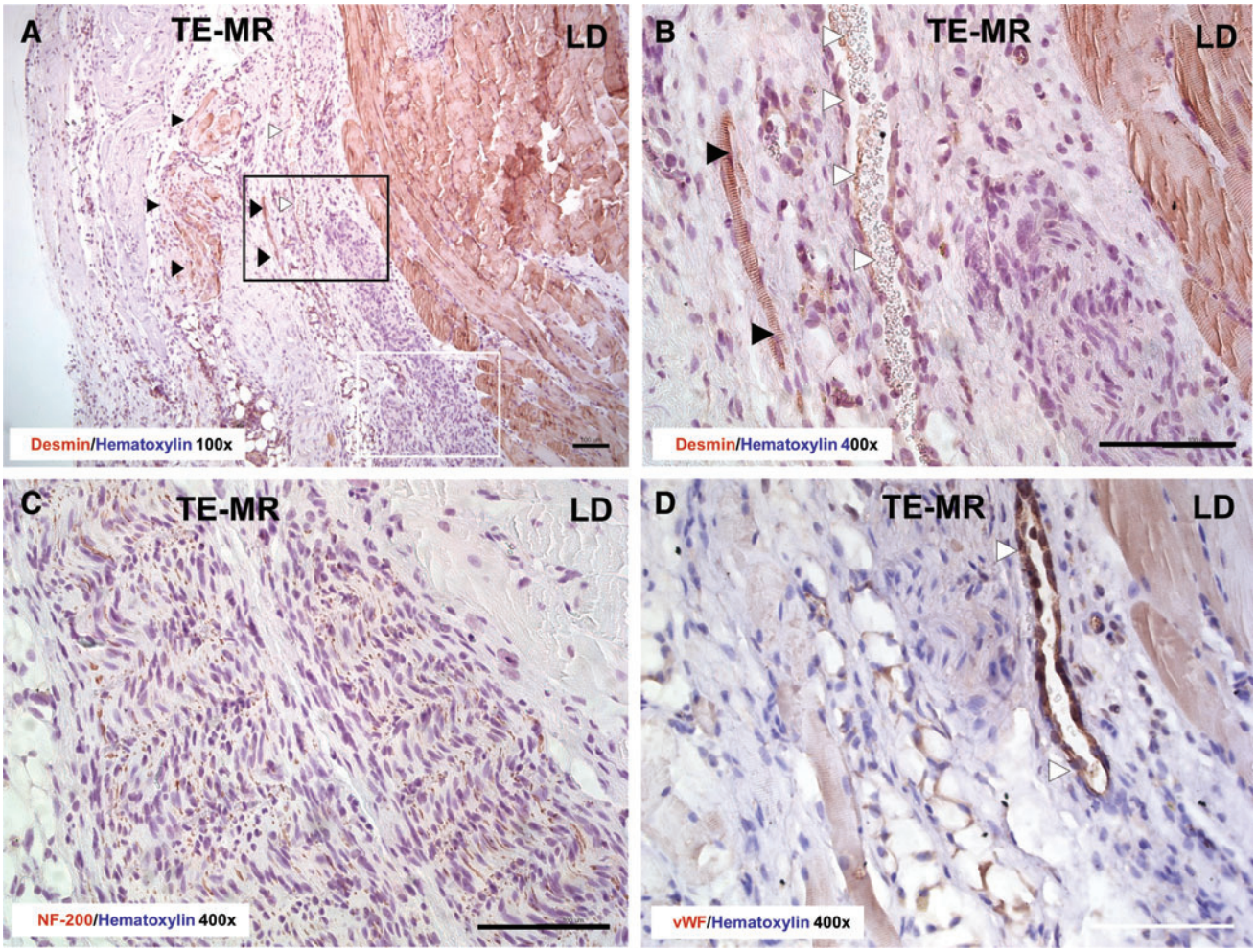

FIG. 5. Histological analysis of R-TE-MR retrieved 2 months after implantation. Immunohistological staining with desmin **(A:** 100×and **B:** 400×**)** provides further evidence for the presence of myofibers (black arrowheads) and blood vessels (white arrowheads) inside the TE-MR construct. NF-200 staining **(C)** indicates the presence of nerves at the interface of the native LD muscle and TE-MR construct. Staining with Von Willebrand factor (vWF) **(D)** demonstrates the presence of blood vessels (white arrowheads) at the interface of the native LD muscle and TE-MR construct. Black rectangle in **A** represents the approximate location of **B** and white rectangle represents approximate location of **C**. All scale bars = 100 μm. Color images available online at www.liebertonline.com/tea

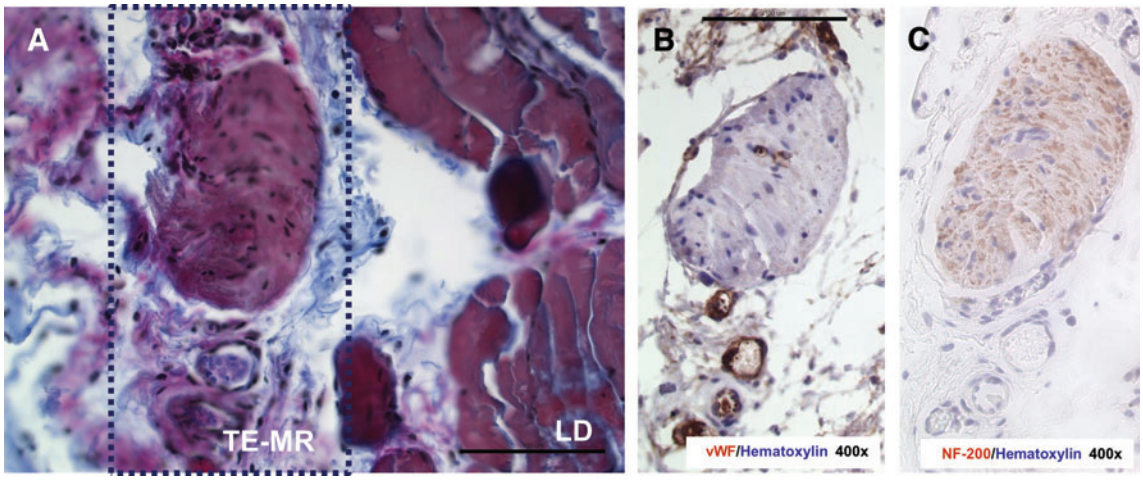

FIG. 6. Formation of neurovascular bundles at the interface of native LD of R-TE-MR retrieved 2 months after implantation. Neurovascular bundle stained with herovici polychrome **(A)**, vWF **(B)** and NF-200 **(C)** in serial sections. Box in **A** represents the area of interest for **B** and **C**. All scale bars = 100 μm. Color images available online at www.liebertonline.com/tea

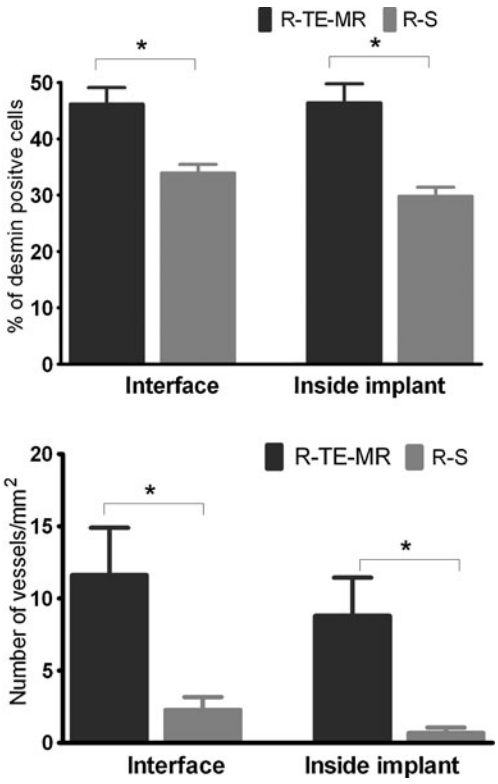

FIG. 7. Quantification of desmin-positive cells and vessel formation in after repair with TE-MR (R-TE-MR) or scaffold alone (R-S, i.e., scaffold with no cells). As illustrated, desmin-positive staining was significantly ($p<0.05$) greater in the R-TE-MR group than in the R-S group both at the interface and inside the implanted construct. Formation of blood vessels in the TE-MR was also significantly ($p<0.05$) greater in R-TE-MR than that of R-S, again, at both the interface and inside the implant; data analyses based on 19 high power field from three different retrieved R-TE-MR tissues and 32 high-power field from four different R-S tissues.

with a time-dependent improvement in the force-producing capacity of the repaired muscle. This fact is highlighted by comparison of the functional recovery observed at 1 and 2 months postimplantation of the TE-MR constructs in Figure 3C and D, respectively. Evidence for this TE-MR-mediated functional improvement at the 2 month time point includes (1) a recovery of maximal absolute isometric force to ~72% of that produced by native LD muscle (Fig. 3D), (2) a similar recovery of maximal isometric specific force to ~66% of that produced by native LD muscle (Fig. 3E), (3) a ~67% to 88% improvement in absolute force across submaximal frequencies compared to no repair (Fig. 3D), (4) a complete recovery of absolute isometric twitch force (1 Hz) compared to native LD muscle, and (5) a restoration of specific caffeine contracture force to ~71% of uninjured LD values for TE-MR-repair LD muscle (Fig. 3F). All of these functional measures occurred 2 months postimplantation of TE-MR, and perhaps most importantly, were significantly greater than the recovery observed in unrepaired muscles (i.e., NR control group) or muscles repaired with scaffold only (i.e., no cells). Taken together, these findings highlight that after creation of a VML injury, LD muscle repaired with TE-MR exhibits improvements in functional quality (i.e., specific force) as well as absolute functional capacity. Moreover, these functional improvements occur not only at maximal levels of stimulation, but also, and potentially more physiologically and clinically relevant,[42,43] at submaximal stimulation levels.

Histological analyses conducted in this study indicate that TE-MR implantation results in skeletal muscle tissue formation that approximates structures typically observed in native muscle. In support of an active cellular regenerative response, desmin-positive multinucleated cells, with and without striations, were detected within the implanted TE-MR, indicative of the presence of myoblasts, myotubes, and myofibers well within the engineered construct (Figs. 4 and 5). Herovici staining also revealed the formation of new collagen fibers along with mature collagen from the scaffold although 2 months postimplantation the amount of scaffold apparently decreased in size based on morphological evaluation upon retrieval. Moreover, NF-200 and vWF staining documented the presence of nerve fibers and blood vessels, respectively (Fig. 5), as well as the presence of neurovascular bundles within the TE-MR construct (Fig. 6). This latter observation is a key finding, as the presence of neurovascular bundles is a prerequisite for sustained functional re-innervation of the engineered/regenerating muscle tissue. To this point, it is important to note that skeletal muscle denervated for ~2 months can exhibit a ~70% reduction in fiber cross-sectional area, with a similar reduction in functional capacity.[44] Thus, although we have not demonstrated the development of functional neuromuscular junctions within the TE-MR in this study, there is sound scientific rationale supporting the supposition that the functional recovery observed with TE-MR implantation is likely achieved in the presence of functional innervation.

As mentioned above, there are distinct approaches being developed for functional restoration of skeletal muscle after VML injury. Of particular interest is the impact of including a cellular component with implanted biocompatible scaffolds. Badylak and colleagues have recently reported that, after 6 months, the implantation of a SIS extracelluar matrix biocompatible scaffold to the site of a musculotendinous injury in dogs resulted in scaffold-localized tissue formation that exhibited the ability to contract when directly stimulated.[25] Similar results were obtained with SIS implantation in a rodent abdominal wall VML injury after direct muscle stimulation *in situ*.[26] In contrast, in a well-designed study aimed specifically to conduct muscle function tests, Merritt *et al*. reported no functional recovery 42 days after implantation of a decellularized muscle matrix in rat gastrocnemius muscle with a VML injury,[29] but did observe significant functional recovery at a similar time postinjury when mesenchymal stem cells were injected into the scaffold site 1 week after implantation.[30]

To further evaluate the impact of a cellular component on functional recovery in our mouse VML injury model, noncell seeded BAM scaffolds were implanted at the site of VML injury in identical fashion to the TE-MR constructs. Two months postimplantation statistical analysis of physiological data revealed no functional recovery in the absence of inclusion of the cellular component. However, despite the lack of functional recovery, significant remodeling and re-cellularization were detected after implantation of the scaffold alone (i.e., no cells). Importantly, quantitative analysis also

revealed a significant increase in the percentage of desmin-positive cells as well as an increase in the number of vessels within the TE-MR construct when compared to implantation of the scaffold/matrix alone (Fig. 7). In addition, with the inclusion of cells we observed a qualitative improvement in phenotypic maturity; as judged by both an increase in the appearance of myotubes and myofibers with striations, as well as an increase in the percentage of desmin-positive cells detected in the TE-MR construct when compared to the scaffold alone. Not surprisingly, varying capacities among biocompatible scaffolds to support skeletal muscle tissue formation and functional restoration have been previously described.[26] Moreover, the functional restoration observed with scaffold-alone implants apparently requires a longer time frame to manifest (e.g., $\geq$6 months).[26,41,45] As such, the functional and histological observations reported here, as well as in the related literature,[27–30,46] illustrate the importance of incorporating a cellular component with implanted scaffolds for more rapid functional recovery of VML injured skeletal muscle in this model (e.g., 2 months).

Future improvements in this technology hinge not only on a more precise understanding of the mechanistic basis for the recovery we observed upon implantation of the TE-MR, but also on the mechanism(s) responsible for the remaining functional deficits. In this regard, an obvious reason for continued force deficits after reparation of VML injury is a reduction in contractile machinery. This rationale is consistent with the extant literature.[25–30,46] More specifically, while varying degrees of putative functional tissue formation have been reported within implanted scaffold matrices, it does not appear, in any instance, that the tissue formation observed is of sufficient volume to completely restore function to muscle after a VML injury.

Further, it is also conceivable that neotissue formation in the scaffold may not exhibit the same functional quality, nor contribute to whole muscle force production in the same manner as native tissue. For example, retrieved LD muscles in this study were exposed to caffeine during organ bath testing as a secondary functional assessment. Because mM concentrations of caffeine stimulate Ca^{2+} release from the SR Ca^{2+} release channel (RyR1), and thereby by-pass upstream components of excitation-contraction coupling, force production during caffeine contracture testing can be inferred as an index of contractile protein content and, when compared to voltage-induced force production, as an index of excitation contraction coupling failure.[32–36,39,47–50] The caffeine contracture forces observed in this study (Fig. 3F) are consistent with the supposition that repair of VML injury with the TE-MR construct, is due, at least in part, to the presence of more contractile machinery; when compared to no repair or scaffold-only repair. However, when considering that the caffeine contracture force relative to voltage-induced force was elevated for the TE-MR construct repair group, it appears that a component of the muscle may be experiencing disruption in the EC coupling process,[21,22,41] which would contribute to voltage-induced force deficits.

Although we did not directly test the mechanistic basis for TE-MR-mediated functional recovery in VML-injured muscle, indirect evidence suggests that a significant portion of the functional recovery is imparted by force delivered via the TE-MR *per se*. Since the functional capacity of skeletal muscle is directly related to muscle fiber cross-sectional area,[44,51–53] another potential mechanism for the functional recovery observed with TE-MR 2 months postimplantation is hypertrophy of the remaining native tissue. While admittedly our study was not designed to directly address LD muscle fiber area or diameter, it is obvious from the histological images of longitudinal sections that we evaluated (following the physiological studies), that there is no clear evidence of the major fiber hypertrophy (over a 50% increase of fiber diameter) in the remaining native portion of the TE-MR repaired LD muscle that would be required to explain the $\sim$60% improvement in force. It is also important to note that compensatory hypertrophy of the native tissue due to surgical ablation-induced overload does not explain the functional recovery of TE-MR repaired LD muscles, as the NR and scaffold-only repaired tissues would also have benefited from this hypertrophic stimulus as well. Nevertheless, it is possible that in addition to the direct functional recovery elicited by the implantation of our TE-MR construct, there may also have been a positive, though indirect, impact of our technology on the repair/regeneration of the remaining portion of the LD muscle. Without question, further investigations are required to more accurately determine the relative proportion of functional recovery due to the direct (i.e., new fiber formation) versus indirect (i.e., cell migration or trophic factors) effect(s) of our technology. Moreover, further study is required to better understand the impact of the host environment (i.e., endogenous stem cells) on the formation of scaffold-localized contractile tissue.

As far as we are aware, there is only a single case report describing the use of a tissue engineering approach for the treatment of a significant muscle defect.[45] In that study, a proprietary acellular biologic extracellular matrix scaffold was used for the treatment of a combat-related VML injury to the quadriceps medialis muscle of a Marine. Despite the encouraging results of this first report, there is still clearly much room for therapeutic improvement. In that regard, the technology described herein represents but a first step in that direction with a scaffold and cell-based alternative strategy. Although our current technology has intrinsic limitations with respect to requisite vascularization and innervation of the larger defects that are characteristic of VML injuries in humans (the ultimate target of this technology), a multi-step layering approach of our scalable sheet-based technology may prove effective, and moreover, there may indeed be other, more immediate clinical indications (e.g., facial nerve paralysis; Bell's Palsy) that are also adequately addressed by this approach. Without question though, utilization of our existing technology for the treatment of the most catastrophic soft tissue injuries suffered by civilians and warfighters may well require the parallel development of additional enabling technologies.

So what can we conclude with respect to the putative mechanistic basis for our current observations? First, it is important to re-emphasize that little or no functional recovery was observed in the absence of treatment with TE-MR in the time frame examined (i.e., compared to the NR and R-S groups). In this scenario, a valid metric (but still, by definition, an underestimate of functional recovery) for assessing the overall degree of recovery of the maximal tetanic response would be to compare the 1 month NR group to the 2 month R-TE-MR group. In fact, whether one considers the extent of functional recovery with respect to the total contractile force,

or normalizes the contraction in terms of specific force, the conclusion is the same, namely, implantation of the TE-MR results in a more than 2-fold increase in maximal contractility. Thus, regardless of the exact mechanistic basis for the observed effects, the current data unequivocally document a consistent and physiologically significant functional recovery after VML injury with our TE-MR technology.

Acknowledgments

This work was supported in part by the Armed Forces Institute for Regenerative Medicine (DoD Contract # W81XWH-08-2-0032), the Orthopaedic Trauma Research Program (USAMRAA ORTP07-07128091) of Department of Defense, Geneva Foundation grant (W81XWH-09-2-0177 awarded to TJW from the United States Army Medical Research Material Command), and NIH USPHS grant AR05735. The authors wish to thank Kristian Andersson, Maja Herco, Sonia Vishwajit, Bimjhana Bishwokarma, and Cathy Mathis for technical assistance and Dr. Robert Grange and Dr. Karl-Erik Andersson for helpful comments and suggestions.

Disclosure Statement

No competing financial interests exist.

References

1. Ambrosio, F., Kadi, F., Lexell, J., Fitzgerald, G.K., Boninger, M.L., and Huard, J. The effect of muscle loading on skeletal muscle regenerative potential: an update of current research findings relating to aging and neuromuscular pathology. Am J Phys Med Rehabil **88,** 145, 2009.
2. Ciciliot, S., and Schiaffino, S. Regeneration of mammalian skeletal muscle. Basic mechanisms and clinical implications. Curr Pharm Des **16,** 906, 2010.
3. Jarvinen, T.A., Jarvinen, T.L., Kaariainen, M., Kalimo, H., and Jarvinen, M. Muscle injuries: biology and treatment. Am J Sports Med **33,** 745, 2005.
4. Lee, J.Y., Qu-Petersen, Z., Cao, B., Kimura, S., Jankowski, R., Cummins, J., Usas, A., Gates, C., Robbins, P., Wernig, A., and Huard, J. Clonal isolation of muscle-derived cells capable of enhancing muscle regeneration and bone healing. J Cell Biol **150,** 1085, 2000.
5. Moss, F.P., and Leblond, C.P. Nature of dividing nuclei in skeletal muscle of growing rats. J Cell Biol **44,** 459, 1970.
6. Snow, M.H. An autoradiographic study of satellite cell differentiation into regenerating myotubes following transplantation of muscles in young rats. Cell Tissue Res **186,** 535, 1978.
7. LaBarge, M.A., and Blau, H.M. Biological progression from adult bone marrow to mononucleate muscle stem cell to multinucleate muscle fiber in response to injury. Cell **111,** 589, 2002.
8. Relaix, F., Rocancourt, D., Mansouri, A., and Buckingham, M. A Pax3/Pax7-dependent population of skeletal muscle progenitor cells. Nature **435,** 948, 2005.
9. Ten Broek, R.W., Grefte, S., and Von den Hoff, J.W. Regulatory factors and cell populations involved in skeletal muscle regeneration. J Cell Physiol **224,** 7, 2010.
10. Holcomb, J.B., Stansbury, L.G., Champion, H.R., Wade, C., and Bellamy, R.F. Understanding combat casualty care statistics. J Trauma **60,** 397, 2006.
11. Lew, T.A., Walker, J.A., Wenke, J.C., Blackbourne, L.H., and Hale, R.G. Characterization of craniomaxillofacial battle injuries sustained by United States service members in the current conflicts of Iraq and Afghanistan. J Oral Maxillofac Surg **68,** 3, 2010.
12. Mazurek, M.T., and Ficke, J.R. The scope of wounds encountered in casualties from the global war on terrorism: from the battlefield to the tertiary treatment facility. J Am Acad Orthop Surg **14,** S18, 2006.
13. Owens, B.D., Kragh, J.F., Jr., Wenke, J.C., Macaitis, J., Wade, C.E., and Holcomb, J.B. Combat wounds in operation Iraqi Freedom and operation Enduring Freedom. J Trauma **64,** 295, 2008.
14. Grogan, B.F., and Hsu, J.R. Volumetric muscle loss. J Am Acad Orthop Surg **19 Suppl 1,** S35, 2011.
15. Norris, B.L., and Kellam, J.F. Soft-tissue injuries associated with high-energy extremity trauma: principles of management. J Am Acad Orthop Surg **5,** 37, 1997.
16. Lawson, R., and Levin, L.S. Principles of free tissue transfer in orthopaedic practice. J Am Acad Orthop Surg **15,** 290, 2007.
17. Khouri, R.K., Cooley, B.C., Kunselman, A.R., Landis, J.R., Yeramian, P., Ingram, D., Natarajan, N., Benes, C.O., and Wallemark, C. A prospective study of microvascular free-flap surgery and outcome. Plast Reconstr Surg **102,** 711, 1998.
18. Lin, C.H., Wei, F.C., Levin, L.S., and Chen, M.C. Donor-site morbidity comparison between endoscopically assisted and traditional harvest of free latissimus dorsi muscle flap. Plast Reconstr Surg **104,** 1070, 1999.
19. Koning, M., Harmsen, M.C., van Luyn, M.J., and Werker, P.M. Current opportunities and challenges in skeletal muscle tissue engineering. J Tissue Eng Regen Med **3,** 407, 2009.
20. Dennis, R.G., Kosnik, P.E., 2nd, Gilbert, M.E., and Faulkner, J.A. Excitability and contractility of skeletal muscle engineered from primary cultures and cell lines. Am J Physiol Cell Physiol **280,** C288, 2001.
21. Levenberg, S., Rouwkema, J., Macdonald, M., Garfein, E.S., Kohane, D.S., Darland, D.C., Marini, R., van Blitterswijk, C.A., Mulligan, R.C., D'Amore, P.A., and Langer, R. Engineering vascularized skeletal muscle tissue. Nat Biotechnol **23,** 879, 2005.
22. Powell, C.A., Smiley, B.L., Mills, J., and Vandenburgh, H.H. Mechanical stimulation improves tissue-engineered human skeletal muscle. Am J Physiol Cell Physiol **283,** C1557, 2002.
23. Shansky, J., Del Tatto, M., Chromiak, J., and Vandenburgh, H. A simplified method for tissue engineering skeletal muscle organoids *in vitro*. In Vitro Cell Dev Biol Anim **33,** 659, 1997.
24. Vandenburgh, H.H., Karlisch, P., and Farr, L. Maintenance of highly contractile tissue-cultured avian skeletal myotubes in collagen gel. In Vitro Cell Dev Biol **24,** 166, 1988.
25. Turner, N.J., Yates, A.J., Weber, D.J., Qureshi, I.R., Stolz, D.B., Gilbert, T.W., and Badylak, S.F. Xenogeneic extracellular matrix as an inductive scaffold for regeneration of a functioning musculotendinous junction. Tissue Eng Part A **16,** 3309, 2010.
26. Valentin, J.E., Turner, N.J., Gilbert, T.W., and Badylak, S.F. Functional skeletal muscle formation with a biologic scaffold. Biomaterials **31,** 7475, 2010.
27. Gamba, P.G., Conconi, M.T., Lo Piccolo, R., Zara, G., Spinazzi, R., and Parnigotto, P.P. Experimental abdominal wall defect repaired with acellular matrix. Pediatr Surg Int **18,** 327, 2002.

28. Kin, S., Hagiwara, A., Nakase, Y., Kuriu, Y., Nakashima, S., Yoshikawa, T., Sakakura, C., Otsuji, E., Nakamura, T., and Yamagishi, H. Regeneration of skeletal muscle using *in situ* tissue engineering on an acellular collagen sponge scaffold in a rabbit model. ASAIO J **53,** 506, 2007.
29. Merritt, E.K., Hammers, D.W., Tierney, M., Suggs, L.J., Walters, T.J., and Farrar, R.P. Functional assessment of skeletal muscle regeneration utilizing homologous extracellular matrix as scaffolding. Tissue Eng Part A **16,** 1395, 2010.
30. Merritt, E.K., Cannon, M.V., Hammers, D.W., Le, L.N., Gokhale, R., Sarathy, A., Song, T.J., Tierney, M.T., Suggs, L.J., Walters, T.J., and Farrar, R.P. Repair of traumatic skeletal muscle injury with bone-marrow-derived mesenchymal stem cells seeded on extracellular matrix. Tissue Eng Part A **16,** 2871, 2010.
31. Moon du G, Christ, G., Stitzel, J.D., Atala, A., and Yoo, J.J. Cyclic mechanical preconditioning improves engineered muscle contraction. Tissue Eng Part A **14,** 473, 2008.
32. Corona, B.T., Rouviere, C., Hamilton, S.L., and Ingalls, C.P. Eccentric contractions do not induce rhabdomyolysis in malignant hyperthermia susceptible mice. J Appl Physiol **105,** 1542, 2008.
33. Corona, B.T., Rouviere, C., Hamilton, S.L., and Ingalls, C.P. FKBP12 deficiency reduces strength deficits after eccentric contraction-induced muscle injury. J Appl Physiol **105,** 527, 2008.
34. Shah, A.J., Pagala, M.K., Subramani, V., Venkatachari, S.A., and Sahgal, V. Effect of fiber types, fascicle size and halothane on caffeine contractures in rat muscles. J Neurol Sci **88,** 247, 1988.
35. Balnave, C.D., and Allen, D.G. Intracellular calcium and force in single mouse muscle fibres following repeated contractions with stretch. J Physiol **488 (Pt 1),** 25, 1995.
36. Ingalls, C.P., Warren, G.L., Williams, J.H., Ward, C.W., and Armstrong, R.B. E-C coupling failure in mouse EDL muscle after *in vivo* eccentric contractions. J Appl Physiol **85,** 58, 1998.
37. Kong, H., Jones, P.P., Koop, A., Zhang, L., Duff, H.J., and Chen, S.R. Caffeine induces Ca2+ release by reducing the threshold for luminal Ca2+ activation of the ryanodine receptor. Biochem J **414,** 441, 2008.
38. Brooks, S.V., and Faulkner, J.A. Contraction-induced injury: recovery of skeletal muscles in young and old mice. Am J Physiol **258,** C436, 1990.
39. Corona, B.T., Balog, E.M., Doyle, J.A., Rupp, J.C., Luke, R.C., and Ingalls, C.P. Junctophilin damage contributes to early strength deficits and EC coupling failure after eccentric contractions. Am J Physiol Cell Physiol **298,** C365, 2010.
40. Ingalls, C.P., Warren, G.L., and Armstrong, R.B. Dissociation of force production from MHC and actin contents in muscles injured by eccentric contractions. J Muscle Res Cell Motil **19,** 215, 1998.
41. Warren, G.L., O'Farrell, L., Summan, M., Hulderman, T., Mishra, D., Luster, M.I., Kuziel, W.A., and Simeonova, P.P. Role of CC chemokines in skeletal muscle functional restoration after injury. Am J Physiol Cell Physiol **286,** C1031, 2004.
42. Adam, A., and De Luca, C.J. Firing rates of motor units in human vastus lateralis muscle during fatiguing isometric contractions. J Appl Physiol **99,** 268, 2005.
43. de Luca, C.J., Foley, P.J., and Erim, Z. Motor unit control properties in constant-force isometric contractions. J Neurophysiol **76,** 1503, 1996.
44. Ashley, Z., Sutherland, H., Lanmuller, H., Russold, M.F., Unger, E., Bijak, M., Mayr, W., Boncompagni, S., Protasi, F., Salmons, S., and Jarvis, J.C. Atrophy, but not necrosis, in rabbit skeletal muscle denervated for periods up to one year. Am J Physiol Cell Physiol **292,** C440, 2007.
45. Mase, V.J., Jr., Hsu, J.R., Wolf, S.E., Wenke, J.C., Baer, D.G., Owens, J., Badylak, S.F., and Walters, T.J. Clinical application of an acellular biologic scaffold for surgical repair of a large, traumatic quadriceps femoris muscle defect. Orthopedics **33,** 511, 2010.
46. Ayele, T., Zuki, A.B., Noorjahan, B.M., and Noordin, M.M. Tissue engineering approach to repair abdominal wall defects using cell-seeded bovine tunica vaginalis in a rabbit model. J Mater Sci Mater Med **21,** 1721, 2010.
47. Moopanar, T.R., and Allen, D.G. Reactive oxygen species reduce myofibrillar Ca2+ sensitivity in fatiguing mouse skeletal muscle at 37 degrees C. J Physiol **564,** 189, 2005.
48. Patel, T.J., Das, R., Friden, J., Lutz, G.J., and Lieber, R.L. Sarcomere strain and heterogeneity correlate with injury to frog skeletal muscle fiber bundles. J Appl Physiol **97,** 1803, 2004.
49. Posterino, G.S., and Dunn, S.L. Comparison of the effects of inorganic phosphate on caffeine-induced Ca2+ release in fast- and slow-twitch mammalian skeletal muscle. Am J Physiol Cell Physiol **294,** C97, 2008.
50. Warren, G.L., Lowe, D.A., Hayes, D.A., Karwoski, C.J., Prior, B.M., and Armstrong, R.B. Excitation failure in eccentric contraction-induced injury of mouse soleus muscle. J Physiol **468,** 487, 1993.
51. Linderman, J.K., and Blough, E.R. Aging does not attenuate plantaris muscle hypertrophy in male Fischer 344 rats. Med Sci Sports Exerc **34,** 1115, 2002.
52. Spector, S.A., Gardiner, P.F., Zernicke, R.F., Roy, R.R., and Edgerton, V.R. Muscle architecture and force-velocity characteristics of cat soleus and medial gastrocnemius: implications for motor control. J Neurophysiol **44,** 951, 1980.
53. Sacks, R.D., and Roy, R.R. Architecture of the hind limb muscles of cats: functional significance. J Morphol **173,** 185, 1982.

Address correspondence to:
George J. Christ, Ph.D.
Wake Forest Institute for Regenerative Medicine
Wake Forest University Baptist Medical Center
Richard H. Dean Biomedical Research Building, Room 442
Medical Center Blvd
Winston-Salem, NC 27157

E-mail: gchrist@wfubmc.edu

Received: November 24, 2010
Accepted: May 5, 2011
Online Publication Date: July 28, 2011